Pergamon

Int. J. Heat Mass Transfer. Vol. 37, No. 13, pp. 1945–1955, 1994

0017-9310/94 $7.00 + 0.00

0017-9310(93)E0117-Y

Wall effects in heat conduction through a heterogeneous material

P. FURMANSKI† and J. M. FLORYAN‡

Department of Mechanical Engineering, The University of Western Ontario, London, Ontario, N6A 5B9, Canada

(*Received* 20 *August* 1993)

Abstract—It is shown that wall effects may significantly alter heat flow through heterogeneous material. These effects can be accurately modelled using the concept of the apparent wall heat transfer coefficient α_w. A method for exact evaluation of α_w is proposed and is used for testing of the ad hoc formulae available in literature. The formula proposed by Kubie (1987) gives the smallest errors and is recommended for use in simplified heat transfer calculations.

1. INTRODUCTION

CHARACTERIZATION of properties of various kinds of heterogeneous materials (porous, granular, suspensions, composites) is very important due to their frequent use in many areas of engineering. One of possible methods is to model these materials macroscopically by assuming that they behave as a continuum characterized by certain effective properties. Determination of the effective properties attracted interest of many investigators and is still the subject of numerous experimental as well as theoretical studies [1, 2].

The macroscopic continuum description of heat conduction in heterogeneous media, in general, has relations similar to those valid for homogeneous media. Certain special effects, such as, for example, nonlocal and memory type behaviour and boundary (wall) effects still remain to be accounted for [3]. While the first two effects are in most instances negligible, the last one can be important even for slow spatially and temporilly varying processes. This can be easily seen in the available experimental data dealing with heat transfer in stagnant beds of solid particles [2, 4]. Measured temperature distribution shows an abrupt change of temperature taking place in the immediate vicinity of the wall. The temperature change propagates usually no more than one particle diameter into the bed and its appearance is attributed to the increased voidage of the medium in the neighbourhood of the wall; it can affect the whole bed in the case of sufficiently narrow beds [5]. In most cases of practical interest the wall effects result in the reduction of the heat flow, which is accounted for by assigning an additional thermal resistance to the wall region of the medium. Determination of the magnitude of this resistance requires estimation of the local porosity in the vicinity of the wall. The available experimental results show that the porosity decreases with distance away from the wall, but the character of the decrease depends on the shape of the particles in the bed. In the case of beds made of regular, equidimensional particles, the porosity decreases in a damped oscillatory manner, while in the case of highly irregular particles it decreases monotonically [6, 7].

The wall effects are also present in other types of heterogeneous materials, such as, for example, composites or porous materials. The role of these effects may be especially important in heat conduction through thin layers, which are frequently utilized in experimental measurements of the effective thermal conductivity.

The inverse of the thermal resistance at the wall is related to the so-called apparent wall heat transfer coefficient, α_w (apparent wall–film coefficient of heat transfer or wall–film coefficient of heat transfer). The available experimental data give large scatter of values of α_w, mainly due to inaccuracy of temperature measurements [2, 8]. Since no general theory is available that could help in rigourously predicting the correct value of α_w, one has to rely either on experimental estimates or on theoretical calculations based on greatly simplified models of unknown accuracy.

The main objective of the present analysis is direct evaluation of the apparent wall heat transfer coefficient α_w. Since it is of interest to correlate α_w with the internal structure of the material, a model of a two-component heterogeneous material consisting of a matrix with randomly distributed small volume fraction spheroidal inclusions is adopted. This model permits investigation of the dependence of α_w on the size of the inclusions (particles), their shapes, orientation and volume fraction, and on the ratio of thermal conductivities of the matrix and the particles. Such a

† Permanent address: Institute of Heat Engineering, Warsaw University of Technology, ul. Nowowiejska 25, 00-665 Warsaw, Poland.

‡ To whom correspondence should be addressed.

NOMENCLATURE

$\mathcal{A}$ configuration of the particles
A_j (A_r) surface area of the jth particle (the reference particle)
$\bar{\bar{A}}$ tensor defined by equation (13)
Bi $\alpha_w d/\lambda_{ef}^{\perp\infty}$, nondimensional apparent wall heat transfer coefficient
$\bar{C}_0, \bar{\bar{C}}_1$ coefficients (vector and tensor) in the linear representation of $\bar{\varphi}$ in equation (18)
d length related to the particle dimension
D_m distance defined below equation (29) and shown in Fig. 3
$\bar{f}$ vector function defined in equation (20)
G Green's function
G_∞ Green's function for infinite medium
H Heavyside step function
$\bar{\bar{K}}$ tensor defined by equation (23)
L particle length
$\bar{n}$ unit vector normal to the surface pointing outwards
n number of particles per unit volume
$p(\bar{r}', \gamma, \varepsilon, R)$ the one particle distribution function defined by equation (29)
$\bar{\bar{P}}$ shape tensor defined by equation (20)
P_l^m, Q_l^m associated Legendre functions of the first and second kind, respectively
q, q_0 components of heat flux vector in the direction perpendicular to the walls for the heterogeneous material and for the pure matrix, respectively
R particle radius
R_T thermal resistance
$\bar{r}_j$ vector describing position of the centre of the reference particle
$\bar{r}' = (x', y', z')$ vector describing position of the reference particle
$\bar{r}^*$ vector connecting centre of the reference particle with centre of its image
$\mathcal{S}$ area of the cross-section of a particle, defined by equation (31)
T temperature
T_w temperature of the wall
T_w^e extrapolated temperature at the wall (Fig. 2)
$\bar{u}_j, \bar{v}_j$ position vectors originating in the centre of the jth particle
$\bar{u}, \bar{v}$ position vectors originating in the centre of the reference particle, $\bar{u} = (u_1, u_2, u_3)$ (Fig. 3)
$\bar{u}^*, \bar{v}^*$ position vectors associated with the image of the reference particle
$(\tilde{u}_1, \tilde{u}_2, \tilde{u}_3)$ local Cartesian coordinate system with origin in the reference particle and with $\tilde{u}_3$ directed along the particle axis of symmetry (Fig. 3)
$\bar{x}, \bar{y}$ position vectors, $\bar{x} = (x, y, z)$, $\bar{y} = (x, y, z)$
$v(z)$ local volume fraction of the particles, $v = \{\theta\}$
v_m volume fraction of the particles in the interior of the slab of heterogeneous material
v_w volume fraction defined by equation (6)
v_∞ volume fraction of the particles far away from the wall
$\tilde{v}$ mean volume fraction of the particles defined below equation (30).

Greek symbols

α_w apparent wall heat transfer coefficient
δ Dirac delta function
Δ thickness of the slab of heterogeneous material
ε particle aspect ratio, $\varepsilon = L/(2R)$
γ angle between the particle axis of symmetry and the z-axis (Fig. 3)
$\Gamma_1, \ldots, \Gamma_6$ functions defined in the Appendix
η, ϑ, ϕ curvilinear, spheroidal coordinate system attached to the centre of the reference particle
η_R value of the coordinate η in the curvilinear, spheroidal system corresponding to the surface of the reference particle
θ characteristic function, equation (12)
$\bar{\bar{\lambda}}_{ef}$ effective thermal conductivity tensor
$\lambda_{ef}^{\perp}$ component of $\bar{\bar{\lambda}}_{ef}$ in the direction perpendicular to the wall
$\lambda_{ef}^{\perp\infty}$ $\lambda_{ef}^{\perp}$ for an infinite domain
λ_1 (λ_0) particle (matrix) thermal conductivity, $\lambda_1' = \lambda_1 - \lambda_0$
σ λ_1/λ_0, relative thermal conductivity, $\sigma' = \lambda_1/\lambda_0 - 1$
$\bar{\varphi}$ microstructure function
$\bar{\omega}$ vector describing orientation of the particle axis of symmetry
$\Omega, \partial\Omega$ volume and surface of the medium
$\{\cdot\}$ ensemble average
$\bar{\nabla}$ (vector) nabla operator
$\bar{a} \cdot \bar{b} = d$ scalar product of vectors $\bar{a}$ and $\bar{b}$
$\bar{a} \cdot \bar{b} = \bar{c}$ scalar product of second-order tensor $\bar{\bar{a}}$ and vector $\bar{b}$
$\bar{a} \cdot \bar{\bar{b}} = \bar{\bar{c}}$ scalar product of second-order tensors $\bar{\bar{a}}$ and $\bar{\bar{b}}$
$\bar{a} \cdot \bar{b} = \bar{\bar{c}}$ affine product of vectors $\bar{a}$ and $\bar{b}$
$\bar{a} \cdot \bar{\bar{b}} \cdot \bar{a} = d$ quadratic form (double scalar product of vector $\bar{a}$ and second-order tensor $\bar{\bar{b}}$).

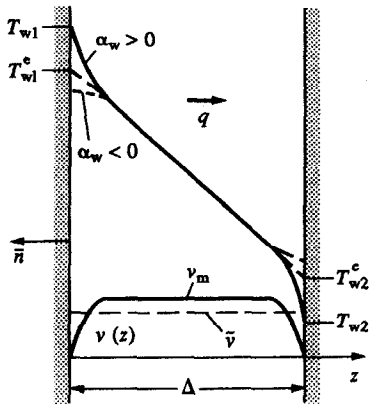

FIG. 1. Typical temperature and volume fraction profiles in a slab of finite thickness made of heterogeneous material.

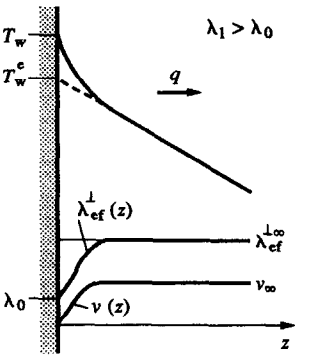

FIG. 2. Distributions of temperature T, effective thermal conductivity $\lambda^{\perp}_{ef}$ and volume fraction v of the particles near the wall bounding heterogeneous material.

model well approximates a wide class of materials used in engineering practice. Results are presented in the form of graphs that could be subsequently used for simplified heat transfer calculations involving heterogeneous materials. The same results are used for assessing the validity of the simplified formulae for α_w available in the literature. Thus, the present analysis provides a firm theoretical justification of the concept of the apparent wall heat transfer coefficient and its practical utilization.

This paper is organized as follows. Section 2 provides description of the apparent wall heat transfer coefficient α_w and two simplified models used for its prediction. Section 3 describes a method for evaluation of the local value of the effective thermal conductivity of a heterogeneous material. This information is used in Section 4 for direct evaluation of α_w. Description of the functional dependence of α_w on various structural parameters characterizing heterogeneous material is given in the same section. Section 5 compares direct evaluation of heat transport through a heterogeneous material with an approximate evaluation utilizing α_w. Section 6 gives a short summary of the main conclusions.

2. THE APPARENT WALL HEAT TRANSFER COEFFICIENT

A typical, experimentally observable [8] temperature distribution in a layer of heterogeneous material exposed to constant temperatures at the opposite walls is shown in Fig. 1. The temperature distribution can be qualitatively divided into a core region, characterized by linearly varying temperature, and two wall layers. Volume fraction of the particles is constant in the core region, and it decreases across the wall layers to reach zero at the walls. The linear temperature in the core region can be extrapolated to the walls giving rise to the extrapolated wall temperatures T^e_{w1}, T^e_{w2}, which are different from the real wall temperatures T_{w1}, T_{w2}.

Heat transfer process in the wall layers can be described by the apparent wall heat transfer coefficient α_w defined as [8]

$$\alpha_w = -(\bar{q}\cdot\bar{n})/(T_w - T^e_w), \tag{1a}$$

where $\bar{q}$ and $\bar{n}$ are the heat flux vector and the unit vector normal to the wall directed outwards, respectively. The available experimental results [2, 5, 8], as well as this study, show that α_w is positive when thermal conductivity of the particles λ_1 is larger than conductivity of the matrix λ_0. Coefficient α_w can take negative values if $\lambda_1 < \lambda_0$. Such values were measured for packed beds [8] and were found in the present study for most of particle shapes. Temperature distributions for positive and negative α_w are shown qualitatively in Fig. 1.

A simplified calculation of heat flow by conduction through heterogeneous material involves summation of three thermal resistances connected in series (two related to the wall effects and one associated with the thickness Δ of the layer of the material, Fig. 1). The expression for the heat flux takes the form

$$q = (T_{w1} - T_{w2})/R_T, \quad R_T = 1/\alpha_w + \Delta/\lambda^{\perp,c}_{ef} + 1/\alpha_w, \tag{1b}$$

where R_T is the total thermal resistance and $\lambda^{\perp,c}_{ef}$ is the effective thermal conductivity of the medium in the core zone. This approach is very attractive for practical (design) calculations due to its simplicity, but its accuracy critically depends on the accurate determination of α_w.

Coefficient α_w can be evaluated by calculating the heat flux directly (taking into account structure of the material) and comparing the resulting expression with equation (1b).

In order to simplify the algebra, we shall consider only a single wall layer as shown in Fig. 2. The effective thermal conductivity of the material is a function of the distance away from the wall and approaches a constant value of $\lambda^{\perp,\infty}_{ef}$ at $z \Rightarrow \infty$ (where temperature T_∞ changes linearly). Similarly, the volume fraction of the particles changes from $v = 0$ at the wall to $v = v_\infty = \text{const}$ at $z \Rightarrow \infty$.

Heat flux, q, flowing through the material in the direction normal to the wall may be calculated by integrating the Fourier equation and taking advantage of the fact that q is constant within the medium. The resulting expression has the form

$$q = (T_w - T_\infty) \Big/ \int_0^\infty \mathrm{d}z/\lambda_{ef}^{\perp}(z). \tag{2}$$

If one assumes that the medium has the same effective thermal conductivity $\lambda_{ef}^{\perp\infty}$ everywhere, then a similar derivation leads to the formula

$$q = (T_w^e - T_\infty) \Big/ \int_0^\infty \mathrm{d}z/\lambda_{ef}^{\perp\infty}(v_\infty). \tag{3}$$

Elimination of T_∞ between equations (2) and (3), and substitution of the resulting expression into the definition of the apparent wall heat transfer coefficient, equation (1), leads to a direct relation between α_w and the effective thermal conductivity. The appropriate dimensionless formula has the form

$$Bi = \alpha_w d/\lambda_{ef}^{\perp\infty} = d \Big/ \int_0^\infty [\lambda_{ef}^{\perp\infty}(v_\infty)/\lambda_{ef}^{\perp}(z) - 1]\,\mathrm{d}z, \tag{4}$$

where d is a reference length scale describing the size of the particles.

Formula (4) is of no use unless distribution of $\lambda_{ef}^{\perp}(z)$ in the vicinity of the wall is known. While theories permitting evaluation of $\lambda_{ef}^{\perp\infty}$ far away from the wall (infinite medium approximation [9]) have been available for quite some time, a method for determination of variations of $\lambda_{ef}^{\perp}(z)$ in the vicinity of the wall has been proposed only very recently [10]. Because of that two ad hoc type approximations for the distribution of $\lambda_{ef}^{\perp}(z)$ have been used in literature. In the first it was assumed that [8]

$$\lambda_{ef}^{\perp}(z) = \begin{cases} \lambda_{ef}^{\perp\infty}(v_w) & \text{for } z \leqslant d/2 \\ \lambda_{ef}^{\perp\infty}(v_\infty) & \text{for } z > d/2, \end{cases} \tag{5}$$

where $\lambda_{ef}^{\perp\infty}(v_w)$ was determined from the expression for the effective thermal conductivity in the infinite medium evaluated for the volume fraction v_w characterizing distribution of the particles in the vicinity of the wall. Quantity v_w was defined as the average volume fraction in a layer adjacent to the wall whose thickness was one-half particle size, i.e.

$$v_w = \int_0^{d/2} v(z)\,\mathrm{d}z/(d/2). \tag{6}$$

The corresponding expression for Bi is

$$Bi = 2/[\lambda_{ef}^{\perp\infty}(v_\infty)/\lambda_{ef}^{\perp\infty}(v_w) - 1]. \tag{7}$$

In the second approximation $\lambda_{ef}^{\perp}(z)$ was assumed to vary according to the formula [1]

$$\lambda_{ef}^{\perp}(z) = \begin{cases} \lambda_{ef}^{\perp\infty}(v) & \text{for } z \leqslant d \\ \lambda_{ef}^{\perp\infty}(v_\infty) & \text{for } z > d \end{cases} \tag{8}$$

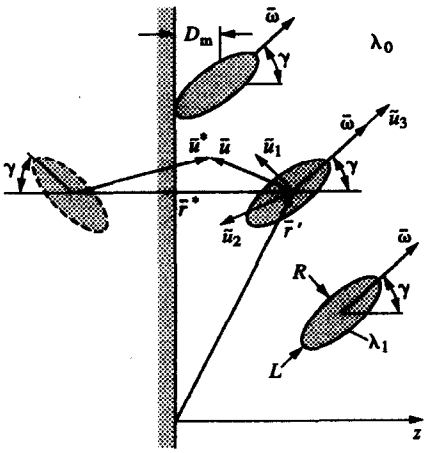

FIG. 3. Characteristic quantities used for analysis of variations of the effective thermal conductivity of the heterogeneous material near the wall.

in which $\lambda_{ef}^{\perp\infty}(v)$ represents the expression describing effective thermal conductivity in the infinite medium, with v_∞ replaced by the local value of the volume fraction $v(z)$ determined by simplified geometrical considerations [11]. The corresponding expression for Bi is

$$Bi = \alpha_w d/\lambda_{ef}^{\perp\infty} = d \Big/ \int_0^\infty [\lambda_{ef}^{\perp\infty}(v_\infty)/\lambda_{ef}^{\perp\infty}(v) - 1]\,\mathrm{d}z. \tag{9}$$

While the accuracy of both approximations discussed above is not known, these expressions are nevertheless widely used because of a lack of viable alternatives.

The ad hoc character of the existing models necessitates careful analysis of the heat transfer process in the vicinity of the wall. We begin this analysis in the next section by describing a theory permitting determination of the actual distribution of $\lambda_{ef}^{\perp}(z)$ in the neighbourhood of the wall. We shall limit our analysis to dilute (small volume fraction) materials only.

3. DETERMINATION OF THE EFFECTIVE THERMAL CONDUCTIVITY NEAR THE WALL

The effective medium theory based on the ensemble averaging concepts is used to determine the effective thermal conductivity of a heterogeneous medium [3]. The ensemble averaging procedures are more powerful than the volume averaging because they are applicable to problems which lack spatial stationarity (in statistical sense), as in the present problem.

Let us consider a half-space made of a heterogeneous material with a wall located at $z = 0$ (Fig. 3). The material consists of a matrix with randomly distributed axisymmetric particles. The particles have spheroidal shape with length L and radius R so that their aspect ratio is $\varepsilon = L/(2R)$. By varying the particle aspect ratio different shapes of the particles may be obtained ranging from flattened disc-like particles

(oblate spheroids with $\varepsilon < 1$) through spheres ($\varepsilon = 1$) to elongated rod-like particles (prolate spheroids with $\varepsilon > 1$). All the particles have the same orientation $\bar{\omega}$ which is described by the orientation angle γ. The angle γ is formed between the particle axis of symmetry and the positive direction of the z-axis (Fig. 3). All particles have the same thermal conductivity λ_1, while the matrix has thermal conductivity λ_0. Both conductivities are assumed to be independent of temperature. It is further assumed that the number of the particles, as defined by their mean volume fraction $\tilde{v}$, is small so their direct interactions are negligible (small volume fraction assumption).

Let us assume that the microstructure length scale ℓ (associated with the variations of the thermal properties of the heterogeneous material) is much shorter than the smallest of macroscopic length scales $\mathscr{L}$ characterizing changes of the average temperature of the material. Then the effective thermal conductivity tensor $\bar{\bar{\lambda}}_{ef}$ may be expressed in terms of the so-called microstructure function $\bar{\varphi}$ by the formula [3]

$$\bar{\bar{\lambda}}_{ef}(\bar{x}) = \lambda_0 \bar{\bar{1}} + \lambda_1' \{\theta(\bar{x}) \bar{\nabla} \bar{\varphi}(\bar{x})\}, \tag{10}$$

where $\bar{\bar{1}}$ and θ are respectively the unit second-order tensor and the characteristic function. The braces ($\{\cdot\}$) represent the ensemble averaging over all possible configuration $\mathscr{A}$ of the particles (i.e. all possible locations, orientations, shapes and dimensions of the particles). The characteristic function θ assumes the value of unity for $\bar{x}$ in the interior of a particle and the value zero otherwise. The microstructure function $\bar{\varphi}$ satisfies the following integrodifferential equation [3]:

$$\bar{\varphi}(\bar{x} \mid \mathscr{A}) = \bar{x} - \lambda_1' \int_{\Omega} \bar{\nabla} G(\bar{x}, \bar{y}) \cdot [\theta(\bar{y} \mid \mathscr{A}) \bar{\nabla} \bar{\varphi}(\bar{y} \mid \mathscr{A}) - \{\theta(\bar{y}) \bar{\nabla} \bar{\varphi}(\bar{y})\}] \, \mathrm{d}\Omega, \tag{11}$$

where $\lambda_1' = \lambda_1 - \lambda_0$ and the integration is carried out over the whole volume Ω occupied by the heterogeneous material.

The analytical expression for the characteristic function θ for the material made of particles distributed in a matrix can be written as

$$\theta(\bar{x} \mid \mathscr{A}) = \sum_{j=1}^{N} \theta_j(\bar{x} \mid \mathscr{A}) = \sum_{j=1}^{N} H[1 - \bar{u}_j \cdot \bar{\bar{A}} \cdot \bar{u}_j], \tag{12}$$

where $\bar{u}_j = \bar{x} - \bar{r}_j$, N is the number of particles in the material, H denotes the Heavyside step function and $\bar{r}_j$ is a position vector describing location of the centre of the jth particle. The tensor $\bar{\bar{A}}$ accounts for the spheroidal shape of the particles and has the form

$$\bar{\bar{A}} = R^{-2} \bar{\bar{1}} + R^{-2}(\varepsilon^{-2} - 1) \bar{\omega} \bar{\omega}, \tag{13}$$

where $\bar{\omega}$ is the vector describing orientation of the particle (Fig. 3). The particles are considered to be indistinguishable because they have the same size and orientation and because they are randomly distributed. One of them is arbitrarily selected to play the role of a reference particle. This particle is denoted by suffix 1 and has a local coordinate system attached to its centre (located at $\bar{r}'$) with $\bar{u}_1 = \bar{u} = \bar{x} - \bar{r}'$. Equation (12) may be utilized to transform equation (11) into

$$\bar{\varphi}(\bar{u} \mid \mathscr{A}) + \lambda_1' \int_{A_1 = A_j} G(\bar{u}, \bar{v}) \bar{\nabla} \bar{\varphi}(\bar{v} \mid \mathscr{A}) \cdot \bar{n} \, \mathrm{d}A_r + \lambda_1' \sum_{j=2}^{N} \int_{A_j} G(\bar{u}_j, \bar{v}_j) \bar{\nabla} \varphi(\bar{v}_j \mid \mathscr{A}) \cdot \bar{n} \, \mathrm{d}A_j = \bar{u} + \lambda_1' \int_{\partial\Omega} G(\bar{u}, \bar{v}) \{\theta(\bar{v}) \bar{\nabla} \bar{\varphi}(\bar{v})\} \cdot \bar{n} \, \mathrm{d}(\partial\Omega), \tag{14}$$

where A_j is the surface of the jth particle and $\bar{n}$ denotes the normal vector external to this surface. The first two terms on the left-hand side of equation (14) refer to the reference particle and the third term describes influence of the neighbouring particles on the microstructure function $\bar{\varphi}$. The right-hand side of the above equation, being the ensemble averaged, is independent of any particular configuration (distribution) of the particles.

The Green's function $G(\bar{u}, \bar{v})$ appearing in equation (14) satisfies the following equations

$$\lambda_0 \bar{\nabla} \cdot G(\bar{u}, \bar{v}) + \delta(\bar{u}, \bar{v}) = 0 \quad \text{for } z > 0 \tag{15}$$

$$G(\bar{u}, \bar{v}) = 0, \quad z = 0. \tag{16}$$

The function $G(\bar{u}, \bar{v})$ may be constructed from the infinite Green's function $G_\infty(\bar{u}, \bar{v})$ by taking advantage of the method of reflections [12], i.e.

$$G(\bar{u}, \bar{v}) = G_\infty(\bar{u}, \bar{v}) - G_\infty(\bar{u}^*, \bar{v}^*; 2z'), \tag{17}$$

where $\bar{u}^*$ and $\bar{v}^*$ are the position vectors whose origins are located at the centre of the (reflected) image of the reference particle located at a distance z' away from the wall (Fig. 3). This particular construction of the Green's function $G(\bar{u}, \bar{v})$ simplifies calculations because it allows the use of systems of coordinates that permit simple modelling of geometry of the particles. In the present study, interest is focused on the spherical and prolate and oblate spheroidal particles which leads to the use of spherical and prolate and oblate spheroidal systems of coordinates.

In order to find the effective thermal conductivity from equation (10) the microstructure function in the interior of the particle is needed (the characteristic function θ vanishes outside the particle). The simplest, acceptable form of the microstructure function $\bar{\varphi}$ is linear, i.e.

$$\bar{\varphi}(\bar{u} \mid \mathscr{A}) = \bar{C}_0(\mathscr{A}) + \bar{\bar{C}}_1(\mathscr{A}) \cdot \bar{u} \tag{18}$$

and it leads to the effective thermal conductivity tensor in the form

$$\bar{\bar{\lambda}}_{ef}(\bar{x}) = \bar{\bar{1}} + \sigma' \{\theta \bar{\bar{C}}_1\}. \tag{19}$$

The vector $\bar{C}_0$ and the second-order tensor $\bar{\bar{C}}_1$ in the above expressions depend on a particular distribution of the particles in the medium. Use of equation (19) requires determination of $\bar{\bar{C}}_1$. This can be done by

substituting the gradient of the microstructure function (20) and expression (19) for the Green's function into equation (14) and dropping the third term on the left-hand side of equation (14). The omitted term describes the influence of the neighbouring particles on the microstructure function in the reference particle and is negligible due to the small volume fraction assumption. The resulting expression contains integrals of the type

$$\int_{A_r} G_r(\bar{u},\bar{v})\bar{n}\,\mathrm{d}A_r = \lambda_0^{-1}\begin{cases}\bar{\bar{P}}\cdot\bar{u} & \text{for points } \bar{u} \text{ inside particle}\\ \bar{\bar{P}}\cdot\bar{f}(\bar{u}) & \text{for points } \bar{u} \text{ outside particle,}\end{cases} \quad (20)$$

where the tensor $\bar{\bar{P}}$ depends only on the shape of the particles. Components of $\bar{\bar{P}}$ and $\bar{f}$ are given in the Appendix for different classes of shapes. Function $\bar{f}(\bar{u}^*)$ describes contributions of the reflected image of the reference particle, with $\bar{u}^*$ denoting the position vector attached to the centre of this image. This function can be replaced around the centre of the reference particle by a linear approximation of the form

$$\bar{f}(\bar{u}^*) = \bar{f}(\bar{r}^*+\bar{u}) = \bar{f}(\bar{r}^*)+\bar{\nabla}\bar{f}(\bar{r}^*)\cdot\bar{u}+\ldots, \quad (21)$$

where $\bar{u}$ is the position vector attached to the centre of the reference particle (Fig. 3). Introduction of equation (21) into the latest form of equation (14) and matching the terms of the same order in $\bar{u}$ leads to a system of two equations for the unknowns $\bar{C}_0$ and $\bar{\bar{C}}_1$. After carrying out derivations described in detail by Furmanski and Floryan [10], $\bar{\bar{C}}_1$ can be expressed in the form

$$C_1(\mathscr{A}) = [\bar{\bar{1}}+\sigma'\bar{\bar{P}}\cdot(\bar{\bar{1}}-\bar{\bar{K}})]^{-1}\cdot[\bar{\bar{1}}-\sigma\{\theta[\bar{\bar{P}}\cdot(\bar{\bar{1}}-\bar{\bar{K}})]\cdot[\bar{\bar{1}}+\sigma'\bar{\bar{P}}\cdot(\bar{\bar{1}}-\bar{\bar{K}})]^{-1}\}]^{-1}, \quad (22)$$

where

$$\bar{\bar{K}} = \bar{\nabla}\bar{f}(\bar{r}^*), \qquad \sigma' = \sigma-1 = \lambda_1/\lambda_0-1. \quad (23)$$

Substitution of expression for $\bar{\bar{C}}_1(\mathscr{A})$ into equation (19) leads to the final formula for the effective thermal conductivity

$$\bar{\bar{\lambda}}_{ef}(\bar{x})/\lambda_0 = \bar{\bar{1}}+\sigma'\{\theta[\bar{\bar{1}}+\sigma'\bar{\bar{P}}\cdot(\bar{\bar{1}}-\bar{\bar{K}})]^{-1}\cdot[\bar{\bar{1}}-\sigma'\{\theta[\bar{\bar{P}}\cdot(\bar{\bar{1}}-\bar{\bar{K}})]\cdot[\bar{\bar{1}}+\sigma'\bar{\bar{P}}\cdot(\bar{\bar{1}}-\bar{\bar{K}})]^{-1}\}]^{-1}. \quad (24)$$

In practical applications, it is the component of the effective thermal conductivity in the direction perpendicular to the wall $\lambda_{ef}^{\perp}$ that is of interest. Its determination is laborious because the principal directions of tensors $\bar{\bar{P}}$ and $\bar{\bar{K}}$ do not in general match. After carrying out the necessary transformations the expression for $\lambda_{ef}^{\perp}$ becomes

$$\lambda_{ef}^{\perp}(z)/\lambda_0 = 1+\frac{\sigma'[\{\theta\Gamma_1\}(1-\sigma'\{\theta\Gamma_2\})-\sigma'\{\theta\Gamma_3\}\{\theta\Gamma_4\}]}{(1-\sigma'\{\theta\Gamma_2\})(1-\sigma'\{\theta\Gamma_5\})-(\sigma')^2\{\theta\Gamma_4\}\{\theta\Gamma_6\}}, \quad (25)$$

where functions $\Gamma_1,\ldots,\Gamma_6$ are given in the Appendix. One may note that, when $z\Rightarrow\infty$, $\lambda_{ef}^{\perp}$ approaches a constant value given by the expression

$$\lambda_{ef}^{\perp\infty}/\lambda_0 = 1+\sigma' v_\infty[(1+\sigma' P_{11})^{-1}\sin^2\gamma/[1-\sigma' v_\infty P_{11}(1+\sigma' P_{11})^{-1}]+(1+\sigma' P_{33})^{-1}\cos^2\gamma/[1-\sigma' v_\infty P_{33}(1+\sigma' P_{33})^{-1}]. \quad (26)$$

Effective application of the formula (25) requires evaluation of the ensemble averages of the type

$$\{\theta(\bar{x})\Gamma_k(\bar{x})\} = \int\theta(\bar{x}|\mathscr{A})\,\Gamma_k(\bar{x}|\mathscr{A})\,p(\mathscr{A})\,\mathrm{d}\mathscr{A}, \quad (27)$$

where $p(\mathscr{A})$ is the probability density function associated with a particular configuration $\mathscr{A}$ of the particles. It is convenient to express the above average in the form [10]

$$\{\theta(\bar{x})\Gamma_k(\bar{x})\} = \int_\Omega\{\theta(\bar{x}|\bar{r}',\gamma,\varepsilon,R)\times\Gamma_k(\bar{x}|\bar{r}',\gamma,\varepsilon,R)\}^*\,p(\bar{r}',\gamma,\varepsilon,R)\,\mathrm{d}\bar{r}', \quad (28)$$

where $\{\theta\Gamma_k\}^*$ is the conditional ensemble average with the centre of the reference particle (of specified dimensions and orientation) located at point $\bar{r}'$ and $p(\bar{r}',\gamma,\varepsilon,R)$ is the density probability function associated with this reference particle. Function $p(\bar{r}',\gamma,\varepsilon,R)$ is known as the 'one-particle distribution function'. In the present case we assume that the particle positions are totally random away from the walls and are strongly influenced by the walls in their vicinity (due to geometrical constraints). The one-particle distribution function may then be approximated by the formula

$$p(\bar{r}',\gamma,\varepsilon,R) = \Omega^{-1}H(z'-D_m) \quad (29)$$

where $D_m = R[(\varepsilon^2-1)\cos^2\gamma+1]^{1/2}$ denotes the minimum permissible distance between the center of the reference particle and the wall (Fig. 3). If expressions (12) and (29) are introduced into the definition (28), and advantage is taken of the facts that the particles are indistinguishable and the functions Γ_k are independent of the coordinates x,y as well as x',y', the formula (29) for the ensemble average may be expressed as

$$\{\theta(z)\Gamma_k(z)\} = \int_0^\infty n\,\Gamma_k(z|z',\gamma,\varepsilon,R)\,\mathscr{S}(z,z',\gamma,\varepsilon,R)\times H\left[1-\frac{|z-z'|}{D_m}\right]H(z'-D_m)\,\mathrm{d}z'. \quad (30)$$

In the above, n is the particle number concentration (i.e. number of particles per unit volume) which is related to the mean particle volume fraction $\bar{v}$ by the expression $n = 3\bar{v}/(4\pi LR^2)$. The symbol $\mathscr{S}$ denotes an area of the cross-section of the reference particle bisected by a plane parallel to the wall and located at

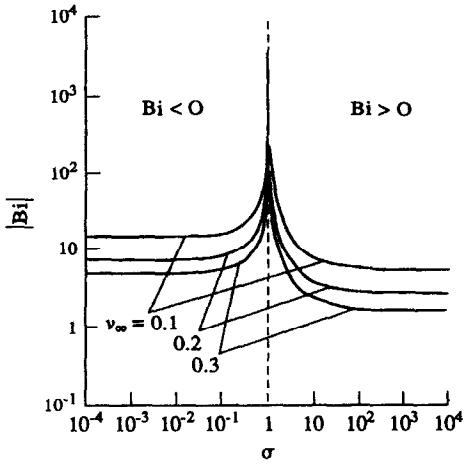

FIG. 4. Variation of the dimensionless wall heat transfer coefficient $Bi = \alpha_w 2D_m/\lambda_{ef}^{\perp}$ as a function of the relative conductivity σ and the mean volume fraction $\bar{v}$ of spherical particles ($\varepsilon = 1$).

a distance z away from it. This area can be calculated from the following formula

$$\mathscr{S}(z, z', \gamma, \varepsilon, R) = \pi R^3 \varepsilon [D_m^2 - (z - z')^2]/D_m^3. \quad (31)$$

4. EVALUATION OF THE APPARENT WALL HEAT TRANSFER COEFFICIENT

The dimensionless wall heat transfer coefficient Bi was calculated directly from equation (4) by making use of the effective thermal conductivity distribution $\lambda_{ef}^{\perp}(z)$ given by equation (25) and the effective thermal conductivity $\lambda_{ef}^{\perp,\gamma}$ for the infinite medium described by formula (26). Results of calculations are shown in Figs. 4–8.

The wall heat transfer coefficient α_w depends on many factors including the size d, the class of shapes, the aspect ratio ε and the volume fraction v_∞ of the particles, and on the ratio σ of the thermal conductivities of the particles and the matrix. The most consise presentation of the results is achieved by adopting the length scale $d = 2D_m$ in the definition of Bi [equation (4)], where D_m is defined below equation (29). One should keep in mind during the following discussion that the wall effects become stronger when $|Bi|$ becomes smaller.

The relative thermal conductivity σ of the particles is the most important factor affecting Bi. A typical plot of Bi vs σ is shown in Fig. 4 for the spherical particles. Bi is positive (and has smaller absolute values) for $\sigma > 1$ and is negative for $\sigma < 1$. When $\sigma \Rightarrow 1$, $|Bi| \Rightarrow \infty$ which corresponds to disappearance of the wall layers. For $\sigma > 100$ (or $\sigma < 0.01$) Bi assumes constant asymptotic values. These results are consistent with the experimental observations of Ofuchi and Kuni [8] and Melanson and Dixon [5].

The second most important factor affecting α_w is the shape of the particles as modelled by the aspect ratio ε (Figs. 5 and 6). The role of this factor is especially pronounced for $\sigma > 1$. In general, the less spherical the particles become, the smaller the value of Bi. The magnitude of Bi is sensitive to the orientation of the particles. These effects are greater for the rod-like particles (Fig. 7) where an increase in γ results in an increase of Bi. The opposite is true for the disc-like particles. Some anomalies in this behaviour are observed when particles are parallel to the wall, i.e. $\gamma \simeq 0$ for the disk-like particles and $\gamma \simeq 90°$ for the rod-like particles (but only for those that are substantially elongated and have a thermal conductivity smaller than the conductivity of the matrix, Fig. 7b).

An increase of the volume fraction of the particles far away from the wall causes the absolute value of the wall heat transfer coefficient to decrease. This decrease is of the order of several percent for v_∞, increasing from 0.05 to 0.33 (Figs. 4 and 6).

The validity of the approximate formulae for Bi cited in the literature has been tested by comparing

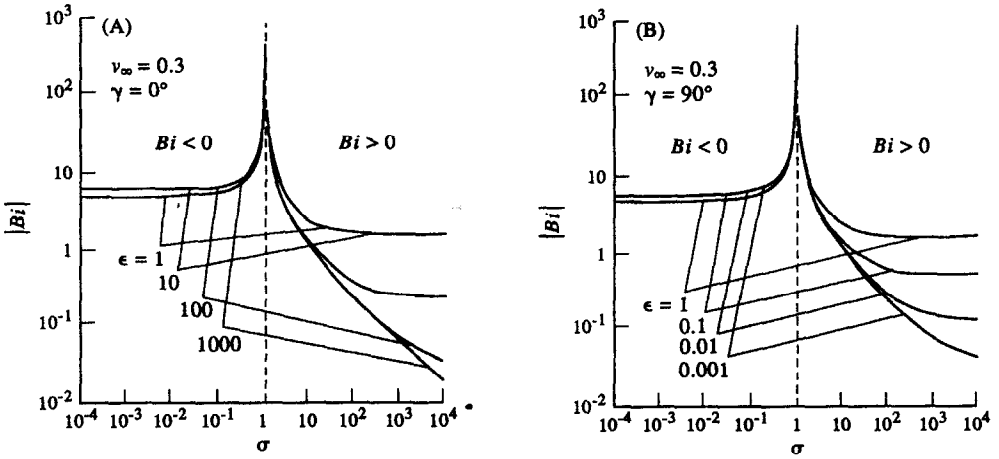

FIG. 5. Variation of the dimensionless wall heat transfer coefficient $Bi = \alpha_w 2D_m/\lambda_{ef}^{\perp,\infty}$ as a function of the particle relative conductivity σ and the the aspect ratio ε: (A) rod-like particles ($\gamma = 0°$), (B) disc-like particles ($\gamma = 90°$).

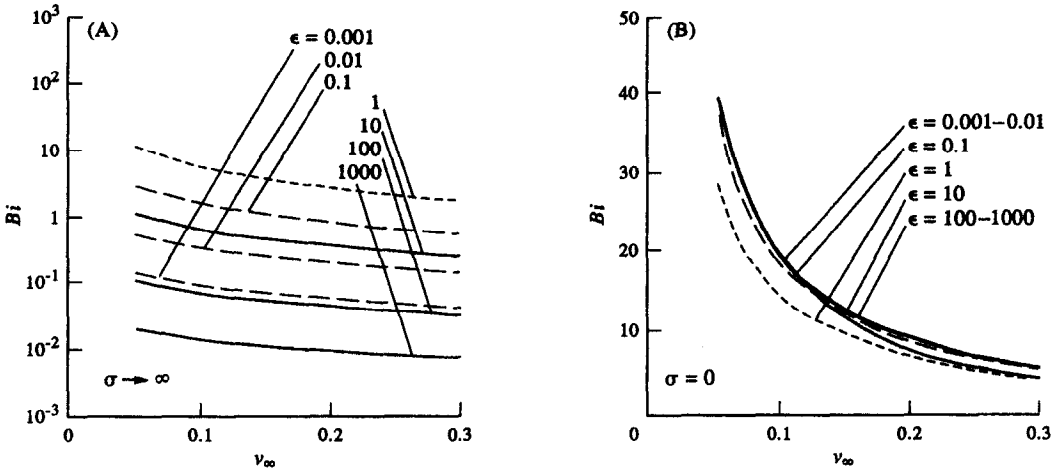

FIG. 6. Variation of the dimensionless wall heat transfer coefficient $Bi = \alpha_w 2D_m/\lambda_{ef}^{\perp\infty}$ as a function of the particle mean volume fraction $\bar{v}$ and the aspect ratio ε: (A) $\sigma \Rightarrow \infty$, (B) $\sigma = 0$. $\gamma = 0°$ for the rod-like particles ($\varepsilon > 1$), $\gamma = 90°$ for the disc-like particles ($\varepsilon < 1$).

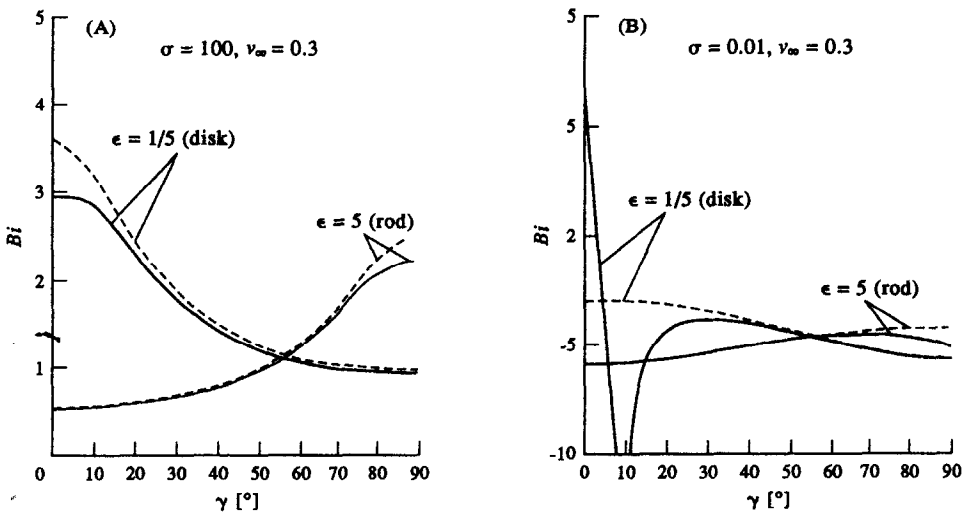

FIG. 7. Variation of the dimensionless wall heat transfer coefficient $Bi = \alpha_w 2D_m/\lambda_{ef}^{\perp\infty}$ as a function of the particle orientation angle γ and the aspect ratio ε: (A) $\sigma = 100$; (B) $\sigma = 0.01$; —— exact formula, equation (4); - - - approximate formula, equation (9).

values of *Bi*s obtained from equations (7) and (9) with the exact solution obtained from equation (4). In general, these formulae give the correct dependence of *Bi* on different parameters and values that are similar to those obtained from equation (4) (Figs. 7 and 8). The agreement is better for the nonspherical particles with ε much different from unity. In most cases equation (9) leads to a better agreement with the exact solution and is, therefore, recommended for use when quick estimates of *Bi* are required.

5. HEAT FLOW THROUGH A SLAB OF HETEROGENEOUS MATERIAL OF FINITE THICKNESS

As noted in Section 1, the concept of the wall heat transfer coefficient α_w has been introduced in order to simplify determination of the heat flow in heterogeneous media. The applicability of this concept will now be demonstrated by calculating heat flux flowing through a slab of heterogeneous material using equation (1b) and comparing these results with the direct solution of the same problem using method described by Furmanski and Floryan [10].

Equation (1b) has to be rearranged for the purpose of calculations. The appropriate substitutions lead to the formula

$$q/q_0 = \frac{\lambda_{ef}^{\perp\infty}(v_m)/\lambda_0}{1+2(d/\Delta)/Bi(v_m)}, \tag{32}$$

where q_0 is the heat flux through the slab made of a pure matrix material and v_m represents the volume fraction of the particles in the interior of the slab (in

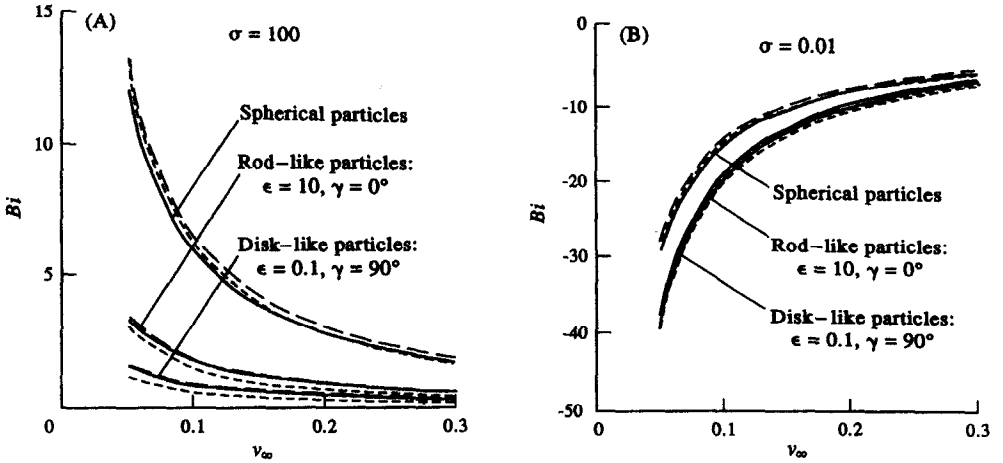

FIG. 8. Variation of the dimensionless wall heat transfer coefficient $Bi = \alpha_w 2D_m/\lambda_{ef}^{\perp\infty}$ as a function of the particle mean volume fraction $\tilde{v}$ and the aspect ratio ε determined using different methods: (A) $\sigma = 100$; (B) $\sigma = 0.01$; —— exact formula, equation (4); --- approximate formula, equation (7); —— approximate formula, equation (9).

the core region away from the walls). For very thick slabs, v_m is practically equal to the mean volume fraction $\tilde{v}$, which is also equal to v_∞, and thus $v_m = v_\infty = \tilde{v}$ in equation (32). This case is easiest to deal with because $\tilde{v}$ is known *a priori*. In the case of thin slabs, volume fraction in the middle of the slab v_m is usually much greater than $\tilde{v}$ (Fig. 1) and has to be calculated for a given distribution of the particles. For the medium consisting of dilute, randomly distributed spheroidal particles (analysed in this paper) this relation can be readily obtained by substituting $\Gamma_k = 1$ in equation (30) and taking account of the finite thickness of the slab, i.e.

$$v_m = 3\tilde{v}/(4\pi LR^2) \times \int_0^\Delta \mathscr{S}(z = \Delta/2, z', \gamma, \varepsilon, R) H\left[1 - \frac{|z - z'|}{D_m}\right] \times (H[z' - D_m] - H[z' - (\Delta - D_m)])\,\mathrm{d}z'. \quad (33)$$

When $2D_m$ is adopted as the reference length scale d, the relation between v_m and $\tilde{v}$ becomes independent of the particle shape, its aspect ratio and its orientation. The functional form of this relation is displayed in Fig. 9 and shows that the value of v_m approaches $\tilde{v}$ for thickness of the slab equal to about 100 particle lengths. For narrow slabs, i.e. for small values of Δ/d, the value of v_m may differ by a factor of up to two from the mean volume fraction $\tilde{v}$.

Analysis of equation (32) reveals the presence of two competing effects arising due to the presence of walls that may lead either to a decrease or to an increase of the overall heat flux. The first effect is obvious, i.e. it is associated with the appearance of the additional wall resistance; it increases q for $Bi < 0$ and it decreases q for $Bi > 0$. The second effect is more subtle and it has to do with the change of $\lambda_{ef}^{\perp\infty}$ in the core region (due to an increase of v_m). This effect can be significant in the case of thin slabs where it can compensate for the increased resistance of the wall layers. The cumulative effect in such slabs cannot be predicted *a priori* and requires detailed calculations.

The results obtained using direct and approximate methods are shown in Figs. 10 and 11. Figure 10 presents dependence of the dimensionless heat flux q/q_0 on the ratio of slab thickness to particle size $\Delta/(2D_m)$ for the spherical particles. The smaller the thickness of the layer relative to the particle size, the greater the reduction of the heat flux due to the wall effects. This reduction is predicted by formula (32) with accuracy sufficient for practical applications beginning with a layer of thickness equal to twice the particle size. A good agreement exists also in the case of nonspherical particles, even for thin layers (thickness of the order of a few particle dimensions) and various particle aspect ratios ε and relative thermal conductivities σ (Fig. 11). It appears that formula (32) may produce an error of practical importance only in the case of thin layers with highly flattened disc-like particles that have $\sigma \ll 1$ and are parallel to the wall.

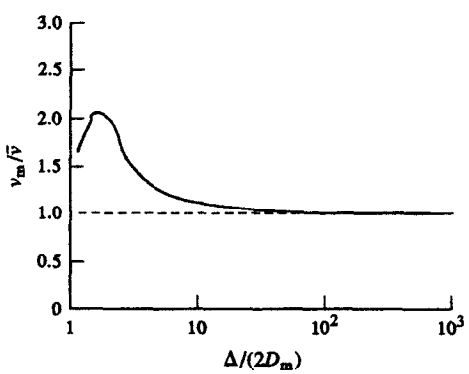

FIG. 9. Relation between the volume fraction v_m in the core region and the mean volume fraction $\tilde{v}$ of the particles as a function of the relative thickness $\Delta/(2D_m)$ of the layer.

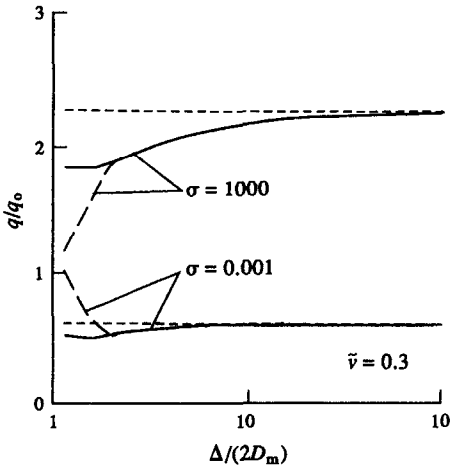

FIG. 10. Variation of the heat flux q/q_0 as a function of the relative thickness $\Delta/(2D_m)$ of the layer of heterogeneous material: —— exact solution [10]; – – – approximate solution, equation (32); – – – asymptotic values for $\Delta/(2D_m) \Rightarrow \infty$.

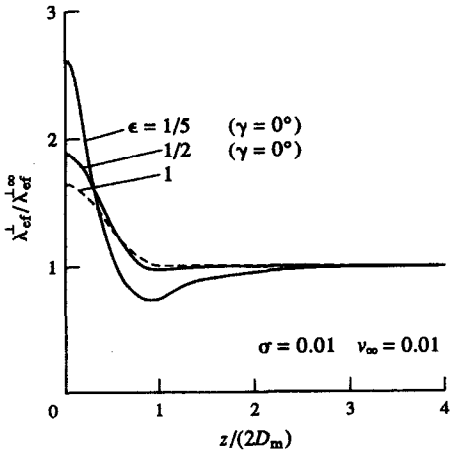

FIG. 12. Variation of the dimensionless effective thermal conductivity $\lambda^{\perp}_{ef}/\lambda^{\perp\infty}_{ef}$ as a function of distance z from the wall and the aspect ratio ε for the relative conductivity $\sigma = 0.01$.

Figure 12 shows distribution of $\lambda^{\perp}_{ef}$ as a function of distance away from the wall for this particular case. It can be seen that the wall layers are sufficiently thick to interact among themselves and to prevent formation of the core region. Formula (32) ceases to be valid under such circumstances.

6. SUMMARY

It is demonstrated that wall effects may significantly alter the heat flow through heterogeneous material. These effects can be accurately modelled using the concept of the apparent wall heat transfer coefficient α_w. A method for evaluation of α_w from the known distribution of the effective thermal conductivity $\lambda^{\perp}_{ef}$ in the case of a material made of a matrix with randomly distributed spheroidal particles is proposed.

The wall heat transfer coefficient α_w may assume both positive and negative values, in agreement with the available experimental measurements. The wall effects become stronger for the lower absolute values of the dimensionless heat transfer coefficient $|Bi|$. Smaller values of $|Bi|$ are obtained by using material consisting of particles and matrix of widely different thermal conductivities, increasing particle volume fraction away from the wall, using more deformed particles (more elongated for the rod-like particles and more flattened for the disc-like particles) and orienting the particles perpendicularly to the wall ($\gamma = 0$ for $\varepsilon > 1$ and $\gamma = 90°$ for $\varepsilon < 1$).

The approximate formulae proposed previously for evaluation of the wall heat transfer coefficient give values of the correct order of magnitude for almost all factors influencing α_w. The formula proposed by Kubie [1] gives values of α_w closest to the exact ones and, therefore, is recommended for use in design calculations even for materials with highly deformed particles and widely varying particle properties.

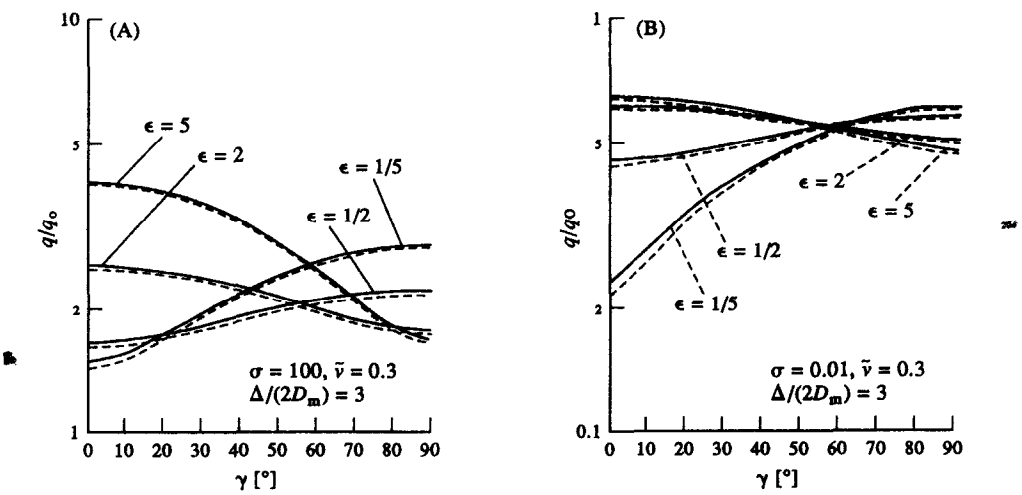

FIG. 11. Variation of the heat flux q/q_0 as a function of the particle orientation angle γ and aspect ratio ε: (A) $\sigma = 100$; (B) $\sigma = 0.01$; —— exact solution [10]; – – – approximate solution, equation (32).

The concept of the wall heat transfer coefficient can be used for calculations of the heat flux beginning with layers of thickness exceeding twice the particle dimension. The predicted heat flux agrees very well with the exact solution. The only exception is the case of narrow layers with highly flattened disc-like particles which have $\sigma \ll 1$ and are parallel to the wall, where the concept of wall heat transfer coefficient ceases to be valid.

Acknowledgements—The authors would like to acknowledge support for this work received from NSERC, Canada and KBN, Poland (grant No. 3-1003-91-01).

REFERENCES

1. J. Kubie, Steady-state conduction in stagnant beds of solid particles. *Int. J. Heat Mass Transfer* **30,** 937–947 (1987).
2. A. G. Dixon, Wall and particle-shape effects on heat transfer in packed beds. *Chem. Engng Commun.* **71,** 217–237 (1988).
3. P. Furmanski, Effective macroscopic description for heat conduction in heterogeneous media. *Int. J. Heat Mass Transfer* **35,** 3047–3058 (1992).
4. S. Yagi and D. Kuni, Studies on heat transfer near wall surfaces in packed beds. *A.I.Ch.E. Jl* **6,** 97–104 (1960).
5. M. M. Melanson and A. Dixon, Solid conduction in low d_t/d_p beds of spheres, pellets and rings. *Int. J. Heat Mass Transfer* **28,** 383–394 (1985).
6. L. H. Roblee, R. M. Baird and J. W. Tierney, Radial porosity variation in packed beds. *A.I.Ch.E. Jl* **4,** 460–464 (1958).
7. V. N. Korolev, N. I. Syromyatnikov and E. M. Tolmachev, The structure of fixed and fluidized granular beds near immersed surfaces. *J. Engng Phys.* **21,** 973–979 (1971).
8. K. Ofuchi and D. Kuni, Heat transfer characteristics of packed beds with stagnant fluids. *Int. J. Heat Mass Transfer* **8,** 749–759 (1965).
9. A. G. Dixon and D. C. Cresswell, Theoretical prediction of effective heat transfer parameters in packed beds. *A.I.Ch.E. Jl* **25,** 663–676 (1979).
10. P. Furmanski and J. M. Floryan, A thermal barrier with adaptive heat transfer characteristics. *ASME J. Heat Transfer* **8,** 302–310 (1994).
11. J. Kubie and J. Broughton, A model of heat transfer in gas fluidized beds. *Int. J. Heat Mass Transfer* **18,** 289–299 (1975).
12. J. D. Jackson, *Classical Electrodynamics*. John Wiley, New York (1975).

APPENDIX

The components of tensor $\bar{\bar{P}}$ and vector $\bar{f}$ may be obtained directly by introducing the infinite Green's function G_∞ expressed in the curvilinear coordinate system (η, ϑ, ϕ), consistent with the particle shape, into the left-hand side of equation (19) and carrying out integration over the angles ϑ and ϕ.

The results are as follows:

(i) for the spherical particles:

$$P_{11} = P_{22} = \tfrac{1}{3} \tag{A1}$$

$$f_1 = -R^3/\eta^2 \sin\vartheta\cos\phi,$$
$$f_2 = -R^3/\eta^2 \sin\vartheta\sin\phi,$$
$$f_3 = -R^3/\eta^2 \cos\vartheta. \tag{A2}$$

(ii) for the rod-like particles:

$$P_{11} = P_{22} = -Q_1^1(\cosh\eta_R)\sinh\eta_R\cosh\eta_R/2,$$
$$P_{33} = Q_1^0(\cosh\eta_R)\sinh^2\eta_R \tag{A3}$$

$$f_1 = [P_1^1(\cosh\eta_R)/Q_1^1(\cosh\eta_R)aQ_1^1(\cosh\eta)\sin\vartheta\cos\phi$$

$$f_2 = [P_1^1(\cosh\eta_R)/Q_1^1(\cosh\eta_R)aQ_1^1(\cosh\eta)\sin\vartheta\sin\phi$$

$$f_3 = [P_1^0(\cosh\eta_R)/Q_1^0(\cosh\eta_R)aQ_1^0(\cosh\eta)\cos\vartheta \tag{A4}$$

where $a = [(L/2)^2 - R^2]^{1/2}$ and $\cosh\eta_R = \varepsilon/(\varepsilon^2-1)^{1/2}$.

(iii) for the disc-like particles:

$$P_{11} = P_{22} = -Q_1^1(i\sinh\eta_R)\sinh\eta_R\cosh\eta_R/2,$$
$$P_{33} = Q_1^0(i\sinh\eta_R)\sinh^2\eta_R \tag{A5}$$

$$f_1 = [P_1^1(i\sinh\eta_R)/Q_1^1(i\sinh\eta_R)aQ_1^1(i\sinh\eta)\sin\vartheta\cos\phi$$

$$f_2 = [P_1^1(i\sinh\eta_R)/Q_1^1(i\sinh\eta_R)aQ_1^1(i\sinh\eta)\sin\vartheta\sin\phi$$

$$f_3 = [P_1^0(i\sinh\eta_R)/Q_1^0(i\sinh\eta_R)aQ_1^0(i\sinh\eta)\cos\vartheta \tag{A6}$$

where $a = [R^2-(L/2)^2]^{1/2}$, $\sinh\eta_R = 1/(1-\varepsilon^2)^{1/2}$ and i is the imaginary unit.

Functions Γ_k appearing in equation (26) may be expressed in the following form:

$$\Gamma_1 = (1+\sigma' U_{11})/W,$$
$$\Gamma_2 = [U_{11}(1+\sigma' U_{33}) - \sigma' U_{13}U_{31}]/W,$$
$$\Gamma_3 = \sigma' U_{31}/W,$$
$$\Gamma_4 = U_{13}/W,$$
$$\Gamma_5 = [U_{33}(1+\sigma' U_{11}) - \sigma' U_{13}U_{31}]/W,$$
$$\Gamma_6 = U_{31}/W, \tag{A7}$$

$$W = (1+\sigma' U_{11})(1+\sigma' U_{33}) - (\sigma')^2 U_{13}U_{31} \tag{A8}$$

where

$$U_{11} = V_1\cos^2\gamma + V_2\sin^2\gamma + V_3\sin\gamma\cos\gamma,$$
$$U_{13} = V_4\cos^2\gamma - V_5\sin^2\gamma + V_6\sin\gamma\cos\gamma,$$
$$U_{31} = V_5\cos^2\gamma - V_4\sin^2\gamma + V_6\sin\gamma\cos\gamma,$$
$$U_{33} = V_2\cos^2\gamma + V_1\sin^2\gamma - V_3\sin\gamma\cos\gamma \tag{A9}$$

and

$$V_1 = P_{11}(1+K_{11}), \qquad V_2 = P_{33}(1+K_{33}),$$
$$V_3 = P_{11}K_{11} + P_{33}K_{33}, \qquad V_4 = P_{11}K_{13},$$
$$V_5 = P_{33}K_{31}, \qquad V_6 = -P_{11}(1+K_{11}) + P_{33}(1+K_{33}). \tag{A10}$$

In the above formulae, $P_{11} = P_{22}$ and P_{33} are the principal components of the tensor $\bar{\bar{P}}$ defined by equations (A1), (A3) and (A5), respectively, and K_{ij} are the components of the tensor $\bar{\bar{K}}$ [equation (23)] expressed in the coordinate system $(\bar{u}_1, \bar{u}_2, \bar{u}_3)$ (Fig. 3).